Magnetic Shape Memory Turns to Nano: Microstructure Controlled Actuation of Free-Standing Nanodisks

NANO MICRO
small

Postfach 10 11 61
69451 Weinheim
Germany
Courier services:
Boschstraße 12
69469 Weinheim
Germany
Tel.: (+49) 6201 606 235
Fax: (+49) 6201 606 500
E-mail: small@wiley.com

WILEY-VCH

Dear Author,

Please correct your galley proofs carefully and return them no more than four days after the page proofs have been received.

Please limit corrections to errors already in the text; cost incurred for any further changes or additions will be charged to the author, unless such changes have been agreed upon by the editor.

The editors reserve the right to publish your article without your corrections if the proofs do not arrive in time.

Note that the author is liable for damages arising from incorrect statements, including misprints.

Please note any queries that require your attention. These are indicated with a Q in the PDF and a question at the end of the document.

Reprints may be ordered by filling out the accompanying form.

Return the reprint order form by fax or by e-mail with the corrected proofs, to Wiley-VCH : small@wiley.com

To avoid commonly occurring errors, **please ensure that the following important items are correct** in your proofs (please note that once your article is published online, no further corrections can be made):

- **Names** of all authors present and spelled correctly
- **Titles** of authors correct (Prof. or Dr. only: please note, Prof. Dr. is not used in the journals)
- **Addresses** and **postcodes** correct
- **E-mail address** of corresponding author correct (current email address)
- **Funding bodies** included and grant numbers accurate
- **Title** of article OK
- All **figures** included
- **Equations** correct (symbols and sub/superscripts)

Corrections should be made directly in the PDF file using the PDF annotation tools. If you have questions about this, please contact the editorial office. The corrected PDF and any accompanying files should be uploaded to the journal's Editorial Manager site.

Author Query Form

WILEY

Journal SMLL

Article smll201803027

Dear Author,

During the copyediting of your manuscript the following queries arose.

Please refer to the query reference callout numbers in the page proofs and respond to each by marking the necessary comments using the PDF annotation tools.

Please remember illegible or unclear comments and corrections may delay publication.

Many thanks for your assistance.

Query No.	Description	Remarks
Q1	Please provide TOC keyword.	
Q2	Please confirm that forenames/given names (blue) and surnames/family names (vermilion) have been identified correctly.	
Q3	Please define RT at the first appearance in the text.	
Q4	Please define HAADF at the first appearance in the text.	
Q5	The citations of 'Methods' have been changed to Experimental Section,' please check.	
Q6	Please define RF at the first appearance in the text.	
Q7	Please define SEM at the first appearance in the text.	
Q8	Please provide the expansion of FEI as it has been cited once in the article.	
Q9	Please check all equations have been correctly typeset.	
Q10	As per the journal style, displayed equations are numbered, so unnumbered displayed equation has been numbered as Equation (1). Please check.	
Q11	Please check book title and editors' names and provide publisher location in ref. (8).	
Q12	Please provide surname for initial abbreviations of authors' names in ref. (33).	

Author: Please confirm that Funding Information has been identified correctly.

Please confirm that the funding sponsor list below was correctly extracted from your article: that it includes all funders and that the text has been matched to the correct FundRef Registry organization names. If a name was not found in the FundRef registry, it may not be the canonical name form, it may be a program name rather than an organization name, or it may be an organization not yet included in FundRef Registry. If you know of another name form or a parent organization name for a "not found" item on this list below, please share that information.

FundRef Name	FundRef Organization Name
Italian Institute of Technology	Istituto Italiano di Tecnologia
University of Parma	Università degli Studi di Parma

COMMUNICATIONS

Q1 xxxx

M. Campanini, L. Nasi, S. Fabbrici, F. Casoli, F. Celegato, G. Barrera, V. Chiesi, E. Bedogni, C. Magén, V. Grillo, G. Bertoni, L. Righi, P. Tiberto, F. Albertini*..... 1803027

Magnetic Shape Memory Turns to Nano: Microstructure Controlled Actuation of Free-Standing Nanodisks

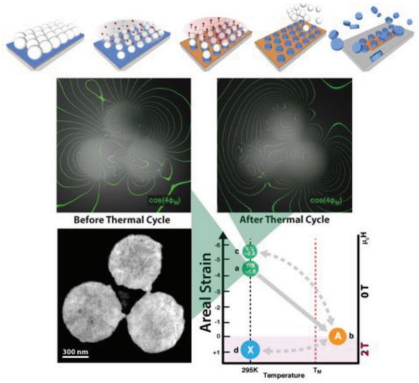

A new actuation mechanism is demonstrated for free-standing Ni_2MnGa nanodisks, with a reversible areal strain tunable in intensity and sign by the application of a magnetic field. The actuation mechanisms are correlated to magnetostructural transformations and visualized by various electron microscopy techniques. The magnetothermal properties of NiMnGa nanodisks pave the way for a new class of temperature-field controlled nanoactuators.

NANO · MICRO small
www.small-journal.com

Magnetic Shape Memory Turns to Nano: Microstructure Controlled Actuation of Free-Standing Nanodisks

Marco Campanini, Lucia Nasi, Simone Fabbrici, Francesca Casoli, Federica Celegato, Gabriele Barrera, Valentina Chiesi, Elena Bedogni, César Magén, Vincenzo Grillo, Giovanni Bertoni, Lara Righi, Paola Tiberto, and Franca Albertini*

Magnetic shape memory materials hold a great promise for next-generation actuation devices and systems for energy conversion, thanks to the intimate coupling between structure and magnetism in their martensitic phase. Here novel magnetic shape memory free-standing nanodisks are proposed, proving that the lack of the substrate constrains enables to exploit new microstructure-controlled actuation mechanisms by the combined application of different stimuli–i.e., temperature and magnetic field. The results show that a reversible areal strain (up to 5.5%) can be achieved and tuned in intensity and sign (i.e., areal contraction or expansion) by the application of a magnetic field. The mechanisms at the basis of the actuation are investigated by experiments performed at different length scales and directly visualized by several electron microscopy techniques, including electron holography, showing that thermo/magnetomechanical properties can be optimized by engineering the martensitic microstructure through epitaxial growth and lateral confinement. These findings represent a step forward toward the development of a new class of temperature-field controlled nanoactuators and smart nanomaterials.

Magnetic shape memory materials were first introduced in 1996 by Ullako et al.[1] who demonstrated magnetic-field-induced strain in NiMnGa Heusler single crystals. Since their discovery, they have gathered a continuously increasing attention for revealing emerging properties that in turn have opened new fields of research and application, such as magnetic actuation,[2–4] ferroic cooling,[5] and energy harvesting.[6,7]

Two main physical properties are at the basis of their challenging phenomenology: a martensitic transformation, i.e., a solid state diffusionless structural transition and magnetically ordered states.[8] The strong coupling between magnetism and structure, driven by the martensitic transformation, gives rise to their multifunctional behavior. "Giant" effects, e.g., magnetomechanical, magnetocaloric, barocaloric/elastocaloric, magnetoresistive, can be induced by external stimuli, such as magnetic field, pressure, stress and their combined application enabling their exploitation in energy-efficient and smart technologies.[2,9–12] Additionally, the coexistence of conventional temperature-induced shape memory effect together with ferromagnetism broadens the range of application.[6,13,14]

In this context, thin films display a great potential with respect to bulk materials for their possible integration in micro/nanosystems for the fabrication of new-concept devices such as actuators, valves, energy harvesters, and solid-state microrefrigerators.[15,16] Nonetheless, the intimate link between magnetic and structural degrees of freedom and the peculiar hierarchical *twin-within-twin* martensitic structure makes epitaxial films a unique platform for the precise control of structure and magnetism from the atomic to the macroscale.

Dr. M. Campanini, Dr. L. Nasi, Dr. S. Fabbrici, Dr. F. Casoli, Dr. V. Chiesi, Dr. V. Grillo, Dr. G. Bertoni, Dr. F. Albertini
IMEM-CNR
Parco Area delle Scienze 37/A, 43124 Parma, Italy
E-mail: franca.albertini@imem.cnr.it
Dr. M. Campanini
Empa
Ueberlandstrasse 129, 8600 Dübendorf, Switzerland
Dr. S. Fabbrici
MIST E-R
via P. Gobetti 101, 40129 Bologna, Italy
Dr. F. Celegato, Dr. G. Barrera, Dr. P. Tiberto
INRIM
Strada delle Cacce 91, 10135 Torino, Italy
The ORCID identification number(s) for the author(s) of this article can be found under https://doi.org/10.1002/smll.201803027.

DOI: 10.1002/smll.201803027

Dr. E. Bedogni, Dr. L. Righi
Dipartimento di Scienze Chimiche
Università di Parma
43121 Parma, Italy
Dr. C. Magén
ICMA
Universidad de Zaragoza-CSIC
50009 Zaragoza, Spain
Dr. C. Magén
LMA
Instituto de Nanociencia de Aragón
Universidad de Zaragoza
50018 Zaragoza, Spain
Dr. V. Grillo
S3-CNR
Via Campi 213A, 41125 Modena, Italy
Dr. G. Bertoni
IIT
Via Morego 30, 16163 Genova, Italy

Recent works have been addressed to microstructure engineering of ferromagnetic shape memory thin films.[17–20] Controlling the microstructure is crucial for the optimization of their functional behavior that is intimately connected to shape memory and magnetomechanical properties, where the twin variants configuration plays a major role. We have recently demonstrated that by an appropriate choice of the growth conditions a fine control of the microstructure is possible in NiMnGa epitaxial thin films.[21]

After the pioneering works of Dong et al.,[22] Jenkins et al.,[23] and Thomas et al.[14] investigating the effects of partial and local release of epitaxial constrain in NiMnGa thin films, we here unveil the effects of lateral confinement in patterned magnetic shape memory thin films and free-standing nanodisks. The possibility to obtain new actuation mechanisms in magnetic shape memory free-standing nanodisks is very promising. Magnetic micro/nanodisks of permalloy and synthetic antiferromagnetic multilayers have been recently proposed in nanomedicine as cellular actuators for new therapeutic approaches, where the cancer cells death is induced by mechanical effects.[24–27] The mechanism at the basis of actuation has a pure magnetic origin, i.e., the rotation/oscillation of nanodisks in alternating magnetic field gradients. In the case of ferromagnetic shape memory nanodisks, after suitable functionalizations, a temperature or magnetic field induced change of shape could enable new applications for manipulating cells and biological molecules.

Within this framework, magnetic shape memory nanodisks are a potential candidate for the production of a new generation of synthetic liquids based on multifunctional materials.

The disks were obtained by a multistep large-scale lithography on epitaxial NiMnGa thin films showing a well-defined microstructure. In **Figure 1**a–f the different steps of the process are shown (for details see the Experimental Section). The process is based on bottom-up self-assembly of polystyrene nanospheres on the surface of the film.[28,29] The disks obtained after sputtering process are successively released from the substrate by selective wet-etching of the Cr underlayer.[30,31] The proposed preparation method is an *easy-to-use*, fast, and low-cost approach to pattern thin films with a wide surface coverage (≈cm^2) very robust in producing nanodisks with a monodispersed size distribution. Additionally, the disks lateral size can be appropriately tuned either by the choice of the polystyrene spheres diameter or changing the process parameters.

The starting specimen was a continuous 75 nm NiMnGa film showing an incommensurate 7 M modulated monoclinic structure (Figure S1, Supporting Information). As shown in the bright field cross-sectional transmission electron microscopy

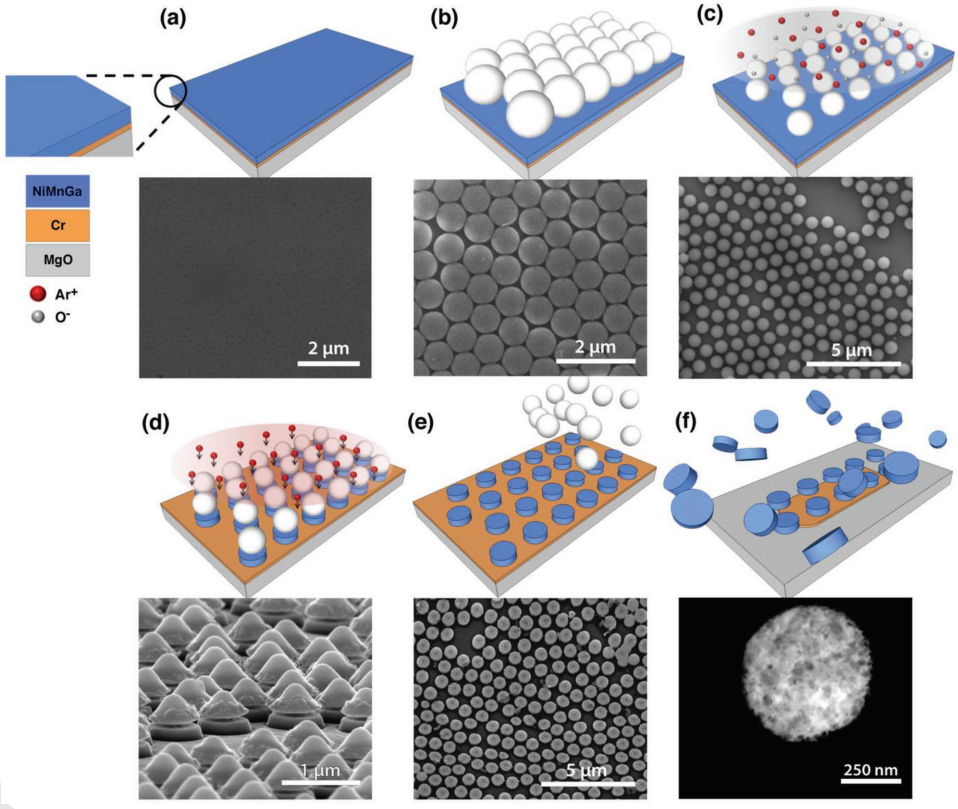

Figure 1. Scheme of the multistep nanofabrication process together with corresponding SEM images acquired at each process stage. a) Continuous 75 nm thick NiMnGa film deposited on a 50 nm thick Cr buffer layer grown onto MgO(001). b) A self-assembled monolayer of polystyrene spheres is deposited onto the surface of the continuous thin film. c) Plasma etching in Ar^+ and O^- gas mixture to reduce polymeric spheres diameter. d) The NiMnGa film is patterned by Ar^+ sputter-etching that selectively removes the material not covered by the polymeric spheres. e) The spheres are removed from the top of NiMnGa disks by ultrasonication. f) The disks are detached from the substrate by a selective wet-etching of the Cr underlayer, obtaining an aqueous suspension of NiMnGa nanodisks.

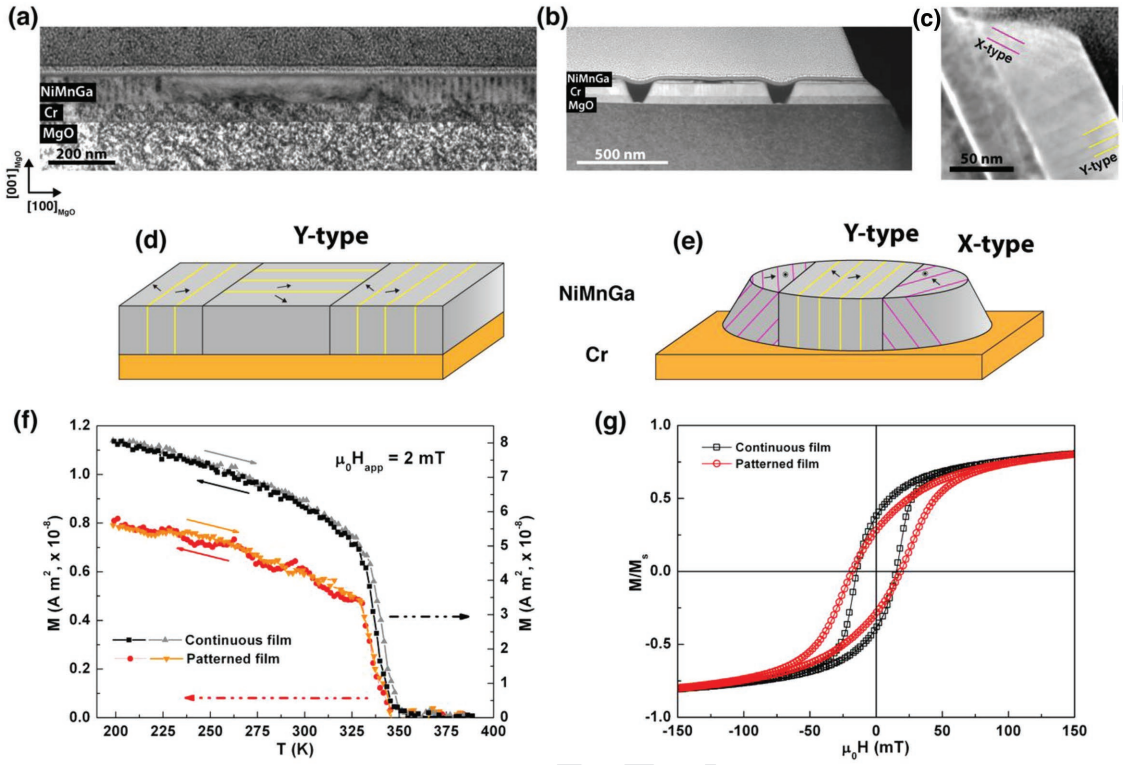

Figure 2. Comparison between martensitic microstructure and magnetic properties in the continuous and patterned thin films. a) Bright Field cross-sectional TEM view of the continuous 75 nm NiMnGa thin film showing Y-type variants only. The scale bar is 200 nm. b) HAADF-STEM image of the patterned film obtained after lithographic processing. The scale bar is 500 nm. c) Magnified view of a region at the border of a disk showing the formation of X-type variants at the edges of the patterned structure. The scale bar is 50 nm. d,e) Schematic representation of the continuous and patterned thin film martensitic structures, showing the formation of different variants (X-type) at the edges of the disks. The lamellae sizes and relative amounts of variants are not in scale. f) Temperature-dependent magnetization evolution acquired under a 2 mT magnetic field applied along the $[100]_{MgO}$ direction in cooling and heating conditions, for both continuous (black and gray symbols) and patterned (red and orange symbols) NiMnGa films. g) In-plane magnetization loops of the NiMnGa continuous (black squares) and patterned (red circles) films under an applied magnetic field along the $[100]_{MgO}$ direction.

(TEM) image in **Figure 2**a, the martensitic microstructure of the continuous film is solely constituted by lamellae oriented along the $[100]_{MgO}$ and $[010]_{MgO}$ directions, named Y-type lamellae. As already pointed out in ref. [21], this configuration of martensitic variants corresponds to a microstructure in which the unique axis lies in the plane of the film, twinned along the equivalent $<110>_{MgO}$ directions. The patterning process induces a slight modification into the martensitic phase and, in particular, into the twin variants configuration. The scanning TEM (STEM) cross-sectional image acquired after lithography, presented in Figure 2b, shows that the shape-profile of the nanodisks resembles that of a truncated cone: the original film thickness gradually reduces at the edges, giving rise to inclined surfaces likely due to the shadowing effect of the capping spheres during the etching process. Remarkably, the nanodisk shape influences microstructure: the inclined edges show a different microstructure (Figure 2c), being constituted of twinning plates oriented at 45° with respect to the substrate (001) (named X-type lamellae) that have been previously observed only in thicker films grown on Cr/MgO or in films without the Cr underlayer.[17,21,23,32] Sketches of the variants configurations for the continuous and patterned films are given in Figure 2d,e.

The magnetic responses of the continuous and patterned films are compared in Figure 2f,g. The continuous film displays an evident and sharp transition from the low temperature ferromagnetic martensitic phase to the high temperature austenitic paramagnetic phase (Figure 2f). The transition displays a narrow hysteresis occurring at T_{MA} = 350 K on heating and at T_{AM} = 348 K on cooling. The magnetic response is not substantially altered by the patterning process that solely determines a slight broadening and shift of the transition temperatures. The continuous and patterned films show similar coercive field values (≈20 mT), testifying a RT martensitic phase for both the samples (Figure 2g). Contrarily, the hysteresis loop slope significantly changes upon patterning due to the modified demagnetizing energy of the disks compared to the continuous film. These measurements prove that the properties at the basis of the multifunctional behavior of this class of materials (i.e., martensitic transformation and the ferromagnetic properties) are preserved in patterned thin films.

Starting from the patterned system, free-standing nanodisks were obtained by wet-etching the sacrificial Cr underlayer. The disks were thoroughly studied by diverse TEM techniques. The analyzed TEM specimens display different mesoscopic configurations of disks, which includes isolated disks, few

interconnected disks, and disks chains. In **Figure 3**a, an HAADF-STEM image of a group of interconnected disks is reported. The bridges between disks are generated by irregularities of the capping layer of the polystyrene spheres that locally affect the efficiency of the sputter-etching process. Stripe contrast due to the different crystallographic orientations of adjacent martensitic plates is visible in the magnified views of the highlighted regions (Figure 3b,c). Figure 3b shows a contrast modulation typical of X-type variant, i.e., 45°-tilted twinning planes. Since the modulation occurring along the [110] direction of the pseudo-orthorhombic setting here lies in the plane of the disk, the easy magnetization axis is twinned from two directions parallel to $[110]_{MgO}$ and $[001]_{MgO}$ directions, respectively.[21] On the contrary, Figure 3c does not show any contrast modulation but twinning planes which are clearly oriented orthogonally to the viewing direction, corresponding to Y-type martensitic variant, i.e., 90°-tilted twinning planes. It is worth noting that, in agreement to what observed for the patterned film, X-type martensitic variants are preferentially observed at the edge of the disks, whereas in the center of the disks the Y-type variants configuration of the continuous thin film is preserved. FFTs of the corresponding high-resolution TEM images for both the regions are given in Figure 3d–f.

The satellite spots typical of 5 M- and 7 M-modulated structure are clearly visible in the X-type zones (Figure 3d,e) due to the modulation vector lying perpendicularly to the observation direction. In Figure 3g the bright-field TEM image of an isolated disk confirms the preferential distribution of X- and Y-type martensitic variants. In the free-standing disks, small areas showing the 5 M structure were also observed. The existence of 5 M modulation can be ascribed to the stress relaxation promoted by the substrate removal. It was recently shown that a tiny stress is needed to trigger the transformation between coexisting structures with different martensitic modulations in Ni-Mn-Ga system and that the 5 M modulation is more stable in a *stress-free* system.[33]

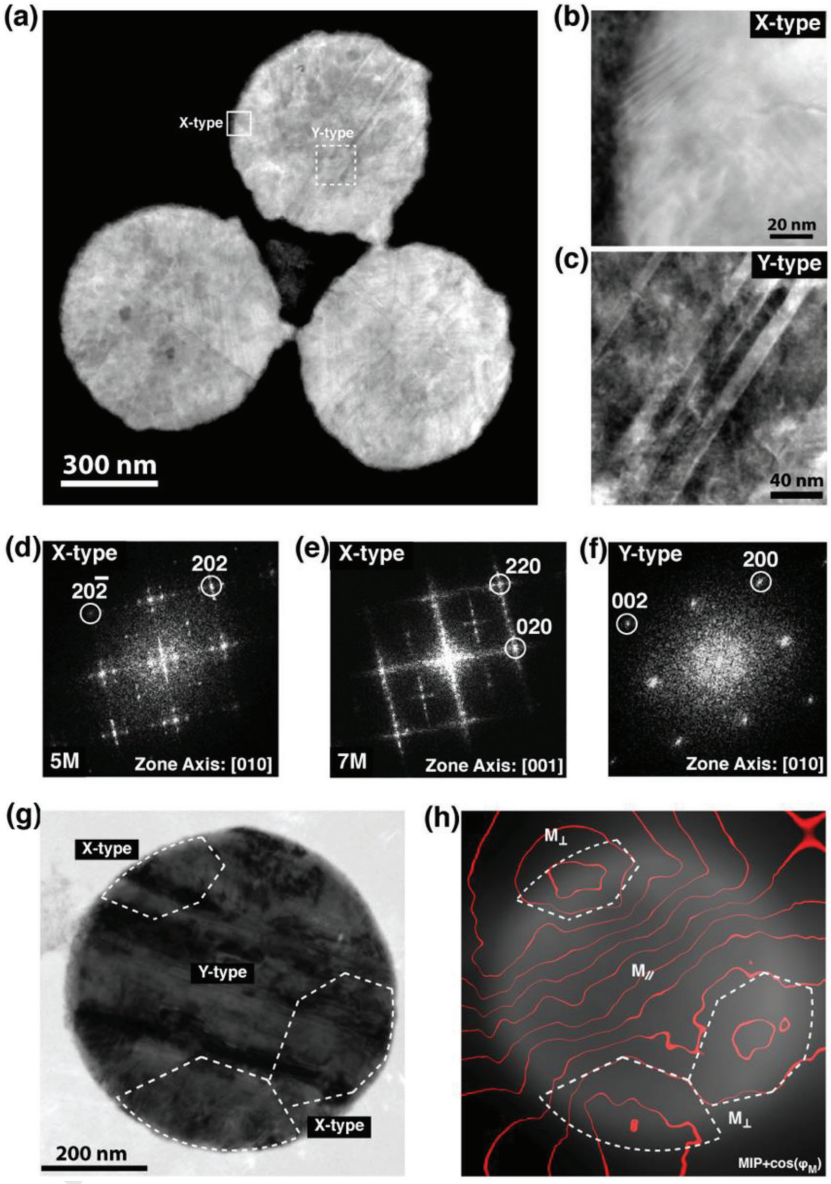

Figure 3. Structure and magnetic configuration of the free standing martensitic disks. a) HAADF-STEM (scale bar: 300 nm) image of free standing disks displaying a martensitic structure that shows both X and Y-type variants. b,c) Magnified views of two regions respectively at the edge and at the center of a martensitic disk (the corresponding regions are marked respectively by the continuous and dashed lines in (a)) showing X-type variants at the edge of the disk and Y-type variants in the central area. The scale bars are 20 nm for (b) and 40 nm for (c). d–f) Corresponding diffractograms that show the different structural orientation of the two areas. For the X-type region the in-plane 5 M/7 M structural modulations produce satellite spots which are visible in the diffractograms. g) Bright-field TEM image of an isolated NiMnGa disk. The scale bar is 200 nm. h) Phase contours of the magnetic phase shift superimposed to the mean inner potential, showing the existence of magnetic domains with an in-plane polarization at the center of the disk and regions with an out-of-plane polarization at the edges, corresponding to Y and X-type variants, respectively.

The magnetic properties of the Ni-Mn-Ga free-standing disks have been investigated by Lorentz microscopy (LM), which enables to study the magnetic structure of individual disks with a spatial resolution of few nanometers (see the Experimental Section for details). Due to the strong correlation between structure and magnetism in martensites, LM is also a fundamental technique to independently confirm the twin variant distribution throughout the nanodisks. In Figure 3h the contour map of the magnetic phase shift is plotted superimposed to the mean inner potential (MIP, see the Experimental Section for details). The central portion of the disk displays an in-plane magnetization with twinned domains, as shown by the more

dense magnetic induction flux line. The lines display undulations that are due to their bending in proximity of the twinning planes. As an example, some twinning planes are marked by continuous white lines in Figure 2f,g. The magnetic configuration is in agreement with the scheme elsewhere described for the Y-type variants.[21] On the contrary, the magnetic induction flux lines at the edges are less dense and close in circles, thus demonstrating that the magnetization is oriented perpendicular to the disk plane as expected from the structural analysis. The LM investigation proves that the magnetic configuration of the free-standing disks differs from the one of the continuous thin films, in which only Y-type variants with in-plane magnetization were observed. Furthermore, we can conclude that the patterning process determines the occurrence of a small portion of X-type variants at the disk edges, while a larger fraction of X-type variants appears after the release of the disks from the substrate. This finding proves that the epitaxial strain relief—in addition to lateral confinement—is a further degree of freedom in free-standing martensitic disks, whose twin variants configuration can reorganize to minimize the *magnetostructural* energy.

In order to achieve a deeper understanding and explore possible actuation mechanisms, we performed a temperature and field-dependent TEM investigation on martensitic disks (**Figure 4**). In particular, the martensitic phase evolution can be properly described considering a disk preferentially constituted by Y-type variants. Herein, we report the results showing the behavior of one selected disk, but information for the overall system properties are also provided, i.e., areal strain and variants distribution ratio (see the Experimental Section for details). In Figure 4a, a RT bright-field TEM image and the relative diffraction pattern of the full disk is reported, in which the twinned reciprocal space cell has been marked in green and the direction of the twinning plane by a white line. The complete transformation from martensite to austenite was obtained by heating the sample up to 513 K, well above the T_{MA} = 350 K. The high temperature phase is recognizable in the bright-field TEM

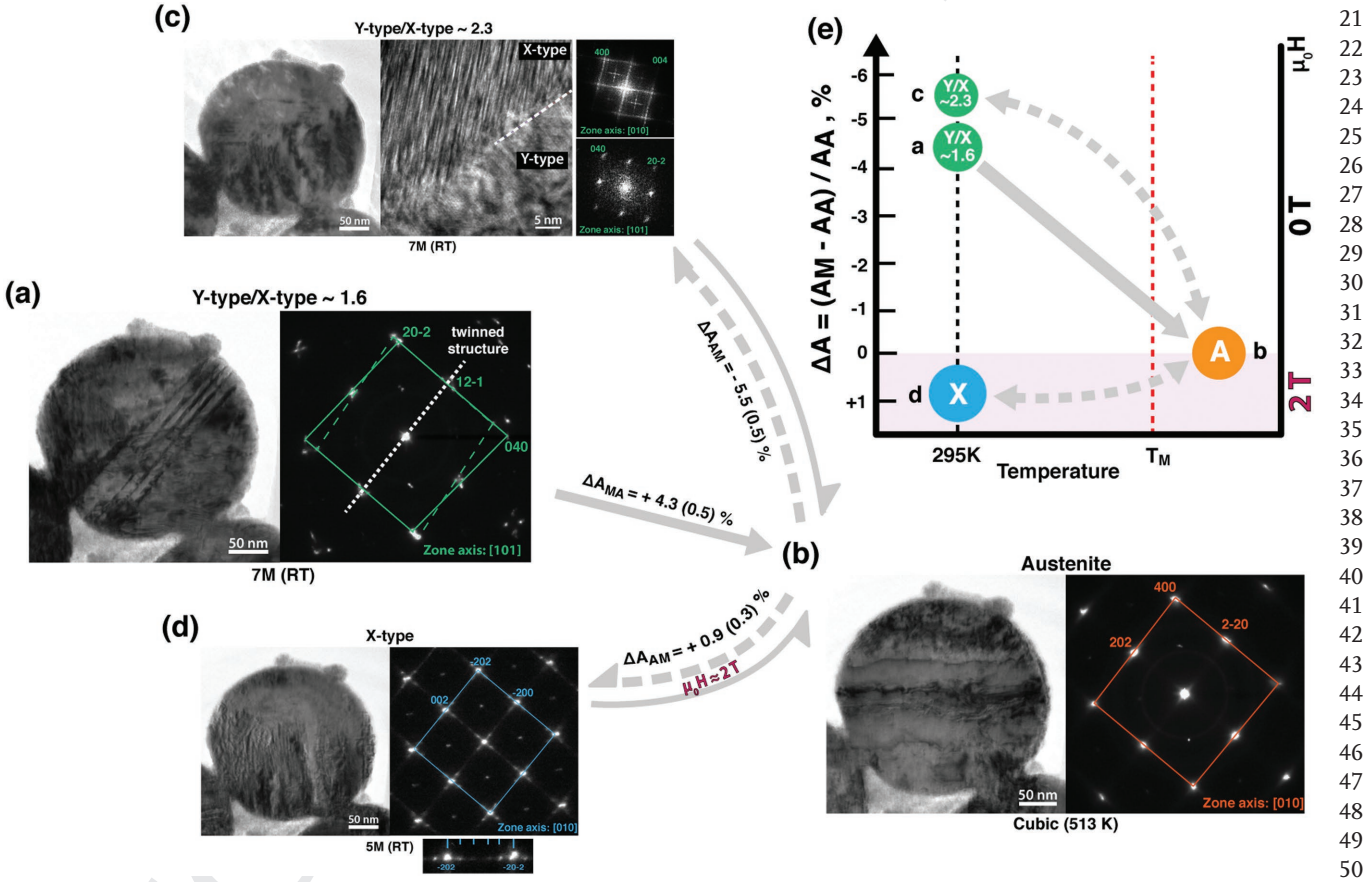

Figure 4. Temperature and field controlled actuation mechanisms in free standing martensitic disks. a) Bright field TEM image of NiMnGa disk together with a diffraction pattern that shows the effect of the twinning planes in Y-type regions. The structure shows a monoclinic symmetry. b) Corresponding bright field TEM image and diffraction pattern taken after heating the sample to 513 K. The crossing of the martensitic phase transformation is marked by the change in the symmetry from monoclinic (as shown in (a)) to cubic. c) Image acquired after cooling down to RT the austenitic phase (shown in (b)), in a magnetic field-free condition ($H = 0$). As shown in the high-resolution TEM image, a new martensitic microstructure showing the coexistence of X- and Y-type variants is obtained upon cooling. d) Cooling down the austenitic phase under an applied magnetic field ($H \approx 2$ T, in the direction perpendicular to the disk) a new martensitic phase showing X-type variants only is obtained, as shown by the diffraction pattern revealing a martensitic structure with the unique axis parallel to the applied magnetic field. From the martensitic states shown in (c) and (d), it is possible to restore the austenitic phase upon heating above T_{MA}. e) Sketch of the areal strain (in %) for the different martensitic phases obtained during the temperature/field-dependent cycle. The areal strains are normalized to the austenitic phase. The scale bar for all the images is 100 nm.

image in Figure 4b, where the contrast features related to the twin variants (i.e., tiny stripes with alternating bright and dark contrast) are lost and the corresponding diffraction pattern has a cubic symmetry, with an estimated lattice parameter of *5.8* Å. We found that the martensitic phase can be restored in the free-standing disks by cooling down the sample below the T_M. In fact, the high-resolution TEM image in Figure 4c highlights a border between two different regions containing X and Y-type variants, as proven by the FFTs of the two different regions. The contrast in the bright-field image of the full disk appears to be different from the one observed in Figure 4a. This result suggests that a new martensitic phase, different from the one displayed at the beginning of the thermal cycle, is generated in the free-standing disk showing that that the lack of epitaxial constraints is effective in making a new martensitic configuration. The phase transformation process is reversible and the austenitic phase can be restored upon heating above T_{MA}.

In order to explore the effects of magnetic field on the martensitic phase transformation in free standing nanodisks, after restoring the austenitic phase we performed a cooling experiment under an applied magnetic field. During in situ TEM experiment, in fact, the sample can be cooled down under a magnetic field of ≈2 T generated by the objective lens of the microscope (see the Experimental Section for details). The lens field is radially symmetric and perpendicular to the plane of the sample and, hence, to the planar view of the disks. The result is shown in Figure 4d in which a new martensitic phase is displayed. The diffraction pattern of the full disk here reported shows a 5 M modulation which lies in the plane of the disk, thus corresponding to a martensitic phase with the unique axis (corresponding to the easy-magnetization direction) oriented along the out-of-plane direction, i.e., parallel to the applied magnetic field. The resulting martensitic microstructure, constituted by only X-type variants, is completely different from the starting one (mainly Y-type variants). Our finding provides the experimental proof that we can actively modify the free-standing nanostructured martensitic phase by different applied stimuli–i.e., temperature and magnetic field.

In addition, we can estimate the average strain generated by such phase transformations. The areal strain was calculated as the average variation in four disks (Figure S3, Supporting Information) taken at the different states across the phase transformation, i.e., for all the states shown in Figure 4a–d. In Figure 4e a sketch of the strain-versus-T phase diagram is reported.

Crossing for the first time T_{MA} (from (a) to (b) in Figure 4), we observe an increase of the area of the system $\Delta A_{MA} = 4.3\% \pm 0.5\%$. Cooling down the sample in a field free environment ($H = 0$)—i.e., transformation from (b) to (c)—we record a reduction of the area of $\Delta A_{AM} = -5.5\% \pm 0.5\%$. The observed difference for the two martensitic phases (i.e., (a) and (c) in Figure 4), whose Y/X variants ratio are ≈1.6 and 2.3, respectively, is a consequence of the different martensitic microstructure accessible upon cycling the phase transformation in the free standing nanodisks. On the contrary, cooling down the sample under the applied magnetic field (≈2 T)—i.e., transition from (b) to (d), in Figure 4—we access a new martensitic phase (showing X-type variants only) giving rise to an expansion $\Delta A_{AM} = 0.9\% \pm 0.3\%$ at the transformation from austenite to martensite.

Three main conclusions therefore follow from our results: i) the nanodisks can be thermally actuated giving rise to a remarkable areal strain (of the order of some %); ii) after thermal cycling the as-released disks, the effect is maximized and a reversible strain (contraction on cooling) of 5.5% is obtained; iii) the areal strain can be inverted in sign (expansion on cooling) by the application of a magnetic field.

These effects are a consequence of the adaptive microstructure of martensite in absence of substrate constraints, which at the transformation selects the microstructural variant distribution able to minimize the magnetic contribution to the total energy. In absence of applied field this contribution is solely due to a magnetostatic term, as proposed by Thomas for free-standing continuous thin films.[14] On the contrary, under an applied field, a Zeeman contribution has to be taken into account in addition to the magnetostatic term.

A direct evidence of the role of the magnetostatic energy at the martensitic transformation of free-standing nanodisks was readily provided by LM experiments. **Figure 5**a shows the

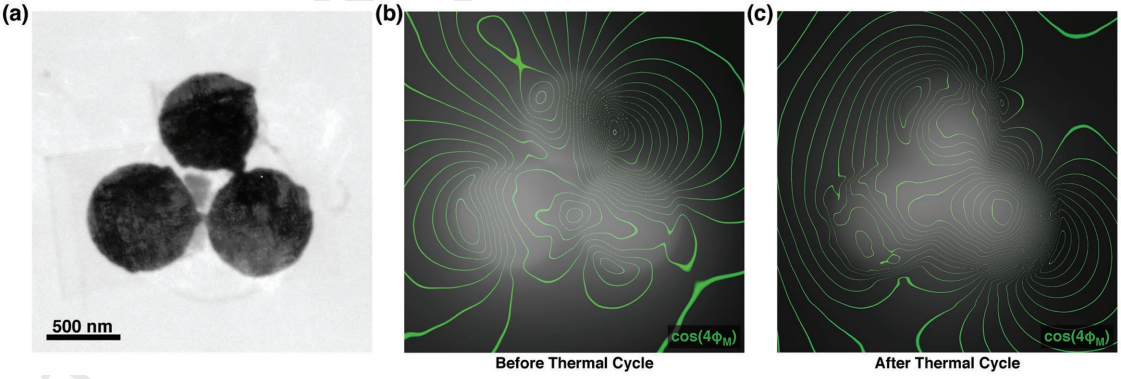

Figure 5. Comparative Lorentz microscopy investigation of the magnetic configuration in the temperature-controlled martensitic phase of free-standing nanodisks. a) Bright field TEM image of a group of three martensitic disks. The scale bar is 500 nm. b) Phase contours of the 5× amplified magnetic phase shift superimposed to the mean inner potential, showing the magnetic configuration of the disks as-detached from the substrate. Such configuration is the one corresponding to the state (a) in Figure 4. c) Corresponding analysis carried out after the thermal cycle performed with $H = 0$, which shows that a new martensitic phase with a different magnetic configuration is obtained (corresponding to the state (c) in Figure 4). The rearrangement of the domains occurs minimizing the stray fields, as proven by the better closure of the magnetic induction flux lines achieved after the thermal cycle.

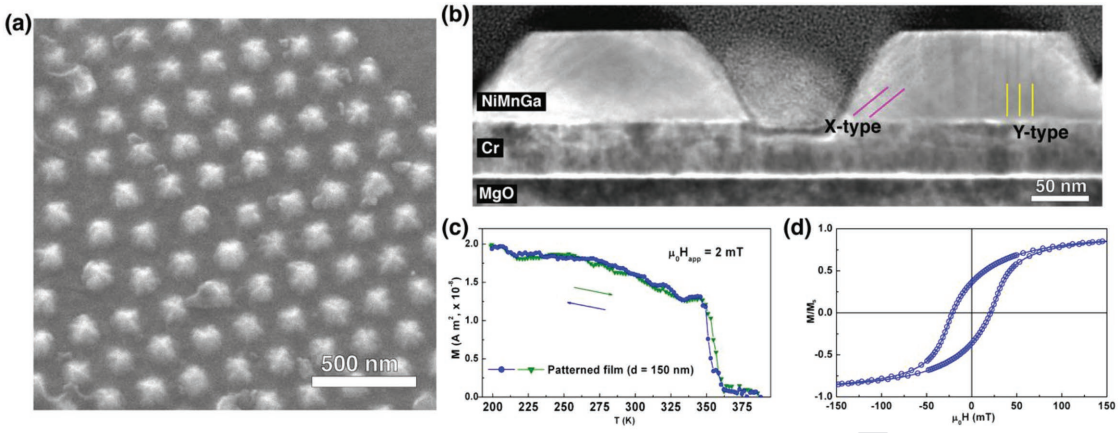

Figure 6. NiMnGa disks after further reduction of lateral dimensions (d = 150 nm) retain the martensitic and magnetic properties. a) SEM image of patterned NiMnGa film, obtained using sphere with reduced lateral dimensions (d = 150 nm). The scale bar is 500 nm. b) HAADF-STEM cross-sectional image of the disks, showing coexistence of X and Y-type variants. The scale bar is 50 nm. c) Temperature-dependent magnetization evolution (cooling: blue circles; heating: green triangles) under a 2 mT applied magnetic field along the $[100]_{MgO}$ direction for the patterned NiMnGa film. d) In-plane magnetization loop with the applied magnetic field along the $[100]_{MgO}$ direction.

change in the magnetic structure of the group of three disks previously introduced in Figure 3a by visualizing the magnetic induction flux lines before and after crossing the structural transformation in absence of an applied field. The comparison of the two maps shown in Figure 5b,c clearly demonstrates that the new twin variants configuration—characterized by a higher amount of Y-type twins—affects the in-plane magnetization of the disks. In particular, the new magnetic structure displays a different geometry of in-plane domains, visible as a change of the density and the direction of the magnetic flux-lines change after the thermal cycle (Figure 5c). Additionally, as a consequence of the reorganization of the twin variants for minimizing the stray fields, the outer extension of the magnetic flux lines is strongly reduced after the thermal cycle.

In summary, nanodisks with a diameter of 650 nm were produced by nanosphere lithography, a cheap and reliable preparation method suitable for large scale production of disks of tailored size. The main properties (i.e., martensitic transformation and ferromagnetic behavior) at the basis of the multifunctional behavior of continuous thin films are not affected by the complex lithographic process. A thorough investigation, achieved by combining different techniques, including Lorentz microscopy (see the Experimental Section for details), was performed to fully characterize the disks at different length scales. The direct effects of lateral confinement and epitaxial stress relaxation on microstructure and magnetism were unveiled and possible actuation mechanisms were directly visualized.

We demonstrated that the martensitic microstructure of free-standing nanodisks is influenced by shape and release of epitaxial constraint, i.e., it is characterized by two differently oriented twin variants (X-type and Y-type) and can be modified by the application of external stimuli, as temperature and magnetic fields. As a consequence, the nanodisks can be thermally actuated giving rise to remarkable areal strain, tunable in sign and intensity by the simultaneous application of a magnetic field. A reversible areal contraction up to 5.5% can be obtained on cooling in zero field, while a 0.9% expansion is obtained by cooling in a perpendicular field.

On the basis of our findings, nanodisks of magnetic shape memory materials appear to be very promising for the realization of a new generation of multifunctional systems such as synthetic liquids and in particular temperature/field controlled suspensions of nanoactuators, whose microstructure can be engineered to tailor the material response for different applications that range from nanoharvesting to nanobioactuation. In this perspective, we have produced patterned thin films constituted by nanodisks of reduced size (diameter of 150 nm) by means of smaller polystyrene nanospheres (i.e., 220 nm), as shown in **Figure 6**a. The martensitic (Figure 6b) and magnetic properties (Figure 6c,d) at the basis of their multifunctional behavior are preserved after the lithographic process. This result demonstrates the possible downscaling of the disk size and it is particularly interesting in the view of tuning properties and broadening the application range of this nanostructured system.

Experimental Section

Film Growth: The Ni_2MnGa (NiMnGa) thin film was grown by RF sputtering at T = 623 K on Cr/MgO(100). The Cr underlayer was epitaxially grown on MgO at the same temperature. Film thickness was 75 nm, while Cr underlayer thickness was 50 nm. The base pressure of the sputtering system was 3×10^{-8} mbar and Ar pressure during the growth was set to 1.5×10^{-2} mbar. The NiMnGa film was sputter deposited from a target with composition $Ni_{49.3}Mn_{27.8}Ga_{22.9}$ (at%). The obtained film composition, as determined by energy dispersive X-rays spectroscopy (EDXS), was $Ni_{53.7}Mn_{22.1}Ga_{24.2}$ (at%).

Nanodisks Fabrication: The multistep process (*nanosphere lithography*) used to fabricate a mask to transfer nanodisks arrays on the film surface is described in the scheme reported in Figure 1 and is based on self-assembly of polystyrene nanospheres. The process stages are here depicted in the sketches while the corresponding film morphology is shown by SEM images acquired at each step of the lithographic process. The starting stage is NiMnGa continuous film shown in Figure 1a. The film surface showing a regular film morphology (not exhibiting surface modulations typical of martensitic plates composed by X-type variants) is visible in the SEM image. The mask for the patterning process was generated by depositing a single layer of polystyrene nanospheres

(Sigma-Aldrich, starting diameter 800 nm) onto the film surface to create an ordered hexagonal array of NPs, as shown in Figure 1b. This is pursued by injecting a droplet containing the NPs on a liquid surface (i.e., deionized water) where they undergo a self-assembling process into an ordered structure. Such an array of nanospheres is subsequently lifted up from water interface using the film itself. The sphere diameter is then reduced by RF plasma (as visible in the SEM image shown in Figure 1c) in a controlled atmosphere obtained as a mixture of Ar and O_2. To end up with close-packed arrays of separated nanodisks, a sputter-etching with Ar ions is performed to etch the film not covered by the polystyrene nanospheres (Figure 1d). Such physical process also strongly modifies the shape of the nanospheres protecting the underneath magnetic film. Polystyrene capping spheres are then removed by sonication and the patterned film is obtained (Figure 1e). The final stage (Figure 1f) consists in a chemical process aimed to dissolve the Cr-underlayer and thus detach the nanodisks from the substrate. Thanks to nanosphere lithography, free-standing nanodisks with mean diameter of 650 nm and thickness of 75 nm are obtained in an aqueous suspension. The aqueous suspension of NiMnGa nanodisks was afterward washed, by iteratively dilution and centrifuging to remove all the residual byproducts of the etching process.

Magnetic Characterizations: Magnetic investigations on the continuous and patterned thin films were performed by means of vibrating sample magnetometer (VSM). In-plane hysteresis loops were measured at RT applying a magnetic field ranging in the interval $-1.7\ \mathrm{T} \leq H \leq 1.7\ \mathrm{T}$ along the $[100]_{MgO}$ direction. The magnetization behavior as a function of temperature was measured in both continuous and patterned films in a temperature interval ranging from 200 to 390 K to investigate the austenite-martensite transformation by using a VSM equipped with a closed cryostat. In particular, the sample was mounted on the VSM tip in order to align the magnetic field along the $[100]_{MgO}$ direction. The measurements were performed under an applied magnetic field of 2 mT after demagnetizing the sample. Low field magnetic measurements as a function of T are particularly useful for studying the magnetic ad structural transitions. In fact an abrupt change of the magnetic susceptibility is expected at the martensitic transformation, arising from the difference of magnetocrystalline anisotropy between the austenitic and martensitic phase. The signal drops to zero at the Curie transition.

The temperature cycle was performed by i) increasing *T* up to 400 K, ii) decreasing T to 200 K, and iii) increasing again T up to 400 K. For all the steps, a constant rate of 0.5 K min^{-1} was set.

Transmission Electron Microscopy: TEM investigations were performed by combining different techniques available on differently configured hardware systems. The TEM samples preparation was carried out by drop casting a few drops of an aqueous suspension containing the free-standing nanodisks on a carbon grid. STEM, conventional TEM imaging and electron diffraction were performed on a JEOL JEM2200FS microscope operated at 200 kV, equipped with an in-column Omega-filter and a silicon drift-detector for EDXS. The temperature-dependent measurements were performed on an aberration-corrected JEOL JEM2200FS microscope operated at 200 kV, using the in situ heating holder. Lorentz microscopy investigations were performed using an aberration corrected FEI Titan^3 80–300 operated at 300 kV and equipped with a Lorentz lens.

The magnetic properties of the NiMnGa free-standing disks were investigated by LM, which enables to study the magnetic structure of individual disks with a spatial resolution of ≈5 nm. Lorentz microscopy was performed at RT turning off the objective lens and using the Lorentz lens to have no field applied on the specimen. The phase of the electron wave was retrieved applying the transport of intensity equation[34] to a Fresnel focal series, whose frames exposition time was set to 1 s and the defocus $\Delta z = 128\ \mu m$. The phase reconstruction process was performed in STEMCELL software.[35] By taking a second focal series after reversing the orientation of the sample, the electrostatic and magnetic contributions to the phase shift can be separated[36,37] following a procedure analogous to the *time-reversal approach*[38] proposed by Tonomura for *off-axis* electron holography. Such separation approach is strictly required to correctly characterize a system displaying a complex shape, e.g., nanodisks, whose geometry is a truncated cone with a local thickness change at the edges, to avoid shape-related artefact in the phase reconstruction process (Figure S2, Supporting Information). Applying the separation method, in fact, the electrostatic contribution (MIP)—related to the thickness distribution for a sample of uniform composition—and the magnetic contribution to the phase shift can be retrieved. It is worth mention that for complex structures constituted by differently oriented magnetic domains, as in the case of martensitic structures, the time-reversal approach represents the sole way in which the separation of the electrostatic and magnetic phase contributions can be performed, since an exact in situ magnetization reversal[39] cannot be obtained applying a magnetic field to the specimen. The TEM in situ experiments were performed setting the heating/cooling rate to 1 K min^{-1} and waiting for 15 min after reaching the desired temperature to permit the system to reach thermal equilibrium and to have a homogenous T over the all TEM grid. During the thermal-cycles (reported in Figure 4a–c) the objective lens was switched off to have the sample in a field-free environment, whilst the in-field cooling was performed with the objective lens on, with an applied magnetic field on the sample ≈2 T parallel to the optical axis of the microscope.[40] The magnetic field is radially symmetric and homogeneous over an area significantly larger than the field of view of the typical TEM images. For small structures like NiMnGa nanodisks whose size is in the sub-micrometric domain, it can be therefore safely assumed that the field is constant over the entire investigated portion of the sample.

Strain Analysis: The deformation of NiMnGa nanodisks induced by martensitic phase transformation in presence or absence of an applied magnetic field was evaluated by measuring the areal strain, defined as

$$\Delta A\,(\%) = \frac{A_M - A_A}{A_A} \times 100 \quad (1)$$

where A_M and A_A are the areas of the disks in the martensitic and austenitic phases, respectively. The areal strain was calculated from the bright field TEM images after images registration.[41] It must be noted that a change in the twin variants configuration is in general an anisotropic deformation, since each twin configuration corresponds to a well-defined orientation of the crystallographic axes of the low symmetry martensitic phase. In order to properly evaluate the average deformations of the martensitic system under the different applied stimuli, the mean areal strains were estimated occurring in a portion of the sample that is representative and significant for the collective behavior of the system. For this purpose, the areal strains as an averaged value over four nanodisks and the error as its standard deviation were calculated. This method represents a convenient way to evaluate the properties of the martensitic system, since the distortion estimated by this approach does not depend on the martensitic structure specific of single nanodisks but resemble the collective behavior of the system.

Supporting Information

Supporting Information is available from the Wiley Online Library or from the author.

Acknowledgements

M.C. thanks Consorzio Spinner for the direct financial support. The authors thanks P. Ranzieri and S. Frabboni for the fruitful discussion for conceiving the in situ experiments, L. Manna for giving access to the electron microscopy facility at Italian Institute of Technology (IIT) in Genova for the temperature-dependent TEM experiments. The authors are grateful to F. Bigi (University of Parma) for giving access to the facilities for the wet-chemistry processing.

Conflict of Interest

The authors declare no conflict of interest.

Keywords

Lorentz microscopy and electron microscopy techniques, magnetic field/temperature actuation of magnetic shape memory materials, magnetic shape memory free standing nanodisks, martensitic microstructure, multifunctional Heusler compounds

Received: July 31, 2018
Revised: September 12, 2018
Published online:

[1] K. Ullakko, J. K. Huang, C. Kantner, R. C. O'Handley, V. V. Kokorin, *Appl. Phys. Lett.* **1996**, *69*, 1966.
[2] R. Kainuma, Y. Imano, W. Ito, Y. Sutou, H. Morito, S. Okamoto, O. Kitakami, K. Oikawa, A. Fujita, T. Kanomata, K. Ishida, *Nature* **2006**, *439*, 957.
[3] A. Sozinov, N. Lanska, A. Soroka, W. Zou, *Appl. Phys. Lett.* **2013**, *102*, 021902.
[4] N. M. Bruno, S. Wang, I. Karaman, Y. I. Chumlyakov, *Sci. Rep.* **2017**, *7*, 40434.
[5] X. Moya, S. Kar-Narayan, N. D. Mathur, *Nat. Mater.* **2014**, *13*, 439.
[6] M. Gueltig, H. Ossmer, M. Ohtsuka, H. Miki, K. Tsuchiya, T. Takagi, M. Kohl, *Adv. Energy Mater.* **2014**, *4*, 1400751.
[7] M. Gueltig, F. Wendler, H. Ossmer, M. Ohtsuka, H. Miki, T. Takagi, M. Kohl, *Adv. Energy Mater.* **2017**, *7*, 1601879.
[8] M. Acet, L. Mañosa, A. Planes, *Handbook of Magnetic Materials* (Eds: K. H. J. Buschow, M. M. Buschow), Elsevier, **2011**, pp. 231–289.
[9] T. Krenke, E. Duman, M. Acet, E. F. Wassermann, X. Moya, L. Mañosa, A. Planes, *Nat. Mater.* **2005**, *4*, 450.
[10] J. Liu, T. Gottschall, K. P. Skokov, J. D. Moore, O. Gutfleisch, *Nat. Mater.* **2012**, *11*, 620.
[11] L. Mañosa, D. González-Alonso, A. Planes, E. Bonnot, M. Barrio, J.-L. Tamarit, S. Aksoy, M. Acet, *Nat. Mater.* **2010**, *9*, 478.
[12] L. Mañosa, A. Planes, *Adv. Mater.* **2017**, *29*, 1603607.
[13] V. Srivastava, Y. Song, K. Bhatti, R. D. James, *Adv. Energy Mater.* **2011**, *1*, 97.
[14] M. Thomas, O. Heczko, J. Buschbeck, Y. W. Lai, J. McCord, S. Kaufmann, L. Schultz, S. Fähler, *Adv. Mater.* **2009**, *21*, 3708.
[15] D. C. Dunand, P. Müllner, *Adv. Mater.* **2011**, *23*, 216.
[16] M. Kohl, M. Gueltig, V. Pinneker, R. Yin, F. Wendler, B. Krevet, *Micromachines* **2014**, *5*, 1135.
[17] P. Ranzieri, S. Fabbrici, L. Nasi, L. Righi, F. Casoli, V. A. Chernenko, E. Villa, F. Albertini, *Acta Mater.* **2013**, *61*, 263.
[18] B. Yang, Y. Zhang, Z. Li, G. Qin, X. Zhao, C. Esling, L. Zuo, *Acta Mater.* **2015**, *93*, 205.
[19] O. Heczko, M. Thomas, J. Buschbeck, L. Schultz, S. Fähler, *Appl. Phys. Lett.* **2008**, *92*, 072502.
[20] Y. Zhang, R. A. Hughes, J. F. Britten, J. S. Preston, G. A. Botton, M. Niewczas, *Phys. Rev. B* **2010**, *81*, 54406.
[21] P. Ranzieri, M. Campanini, S. Fabbrici, L. Nasi, F. Casoli, R. Cabassi, E. Buffagni, V. Grillo, C. Magén, F. Celegato, G. Barrera, P. Tiberto, F. Albertini, *Adv. Mater.* **2015**, *27*, 4760.
[22] J. W. Dong, J. Q. Xie, J. Lu, C. Adelmann, C. J. Palmstrom, J. Cui, Q. Pan, T. W. Shield, R. D. James, S. McKernan, *J. Appl. Phys.* **2004**, *95*, 2593.
[23] C. A. Jenkins, R. Ramesh, M. Huth, T. Eichorn, P. Pörsch, H. J. Elmers, *Appl. Phys. Lett.* **2008**, *93*, 234101.
[24] D.-H. Kim, E. A. Rozhkova, I. V Ulasov, S. D. Bader, T. Rajh, M. S. Lesniak, V. Novosad, *Nat. Mater.* **2010**, *9*, 165.
[25] S. Leulmi, X. Chauchet, M. Morcrette, G. Ortiz, H. Joisten, P. Sabon, T. Livache, Y. Hou, M. Carriere, S. Lequien, B. Dieny, *Nanoscale* **2015**, *7*, 15904.
[26] T. Vemulkar, E. N. Welbourne, R. Mansell, D. C. M. C. Petit, R. P. Cowburn, *Appl. Phys. Lett.* **2017**, *110*, 042402.
[27] Y. Cheng, M. E. Muroski, D. C. M. C. Petit, R. Mansell, T. Vemulkar, R. A. Morshed, Y. Han, I. V Balyasnikova, C. M. Horbinski, X. Huang, L. Zhang, R. P. Cowburn, M. S. Lesniak, *J. Controlled Release* **2016**, *223*, 75.
[28] J. C. Hulteen, R. P. Van Duyne, *J. Vac. Sci. Technol., A* **1995**, *13*, 1553.
[29] P. Tiberto, F. Celegato, G. Barrera, M. Coisson, F. Vinai, P. Rizzi, *Sci. Technol. Adv. Mater.* **2016**, *17*, 462.
[30] A. Backen, S. R. Yeduru, M. Kohl, S. Baunack, A. Diestel, B. Holzapfel, L. Schultz, S. Fähler, *Acta Mater.* **2010**, *58*, 3415.
[31] T. Eichorn, R. Hausmanns, G. Jakob, *Acta Mater.* **2011**, *59*, 5067.
[32] A. Backen, S. R. Yeduru, A. Diestel, L. Schultz, M. Kohl, S. Fähler, *Adv. Eng. Mater.* **2012**, *14*, 696.
[33] L. H., D. Y. C., Z. L. W., Z. H. N., Y. H. D., Y. Z., Y. R., Y. D. Wang, *J. Phys. D: Appl. Phys.* **2015**, *48*, 265304.
[34] V. V. Volkov, Y. Zhu, *Phys. Rev. Lett.* **2003**, *91*, 43904.
[35] V. Grillo, F. Rossi, *Ultramicroscopy* **2013**, *125*, 112.
[36] E. Humphrey, C. Phatak, A. K. Petford-Long, M. De Graef, *Ultramicroscopy* **2014**, *139*, 5.
[37] M. Campanini, R. Ciprian, E. Bedogni, A. Mega, V. Chiesi, F. Casoli, C. de Julian Fernandez, E. Rotunno, F. Rossi, A. Secchi, F. Bigi, G. Salviati, C. Magen, V. Grillo, F. Albertini, *Nanoscale* **2015**, *7*, 7717.
[38] A. Tonomura, T. Matsuda, J. Endo, T. Arii, K. Mihama, *Phys. Rev. B* **1986**, *34*, 3397.
[39] R. E. Dunin-Borkowski, M. R. McCartney, D. J. Smith, S. S. P. Parkin, *Ultramicroscopy* **1998**, *74*, 61.
[40] L. A. Rodríguez, C. Magén, E. Snoeck, C. Gatel, L. Marín, L. Serrano-Ramón, J. L. Prieto, M. Muñoz, P. A. Algarabel, L. Morellon, J. M. De Teresa, M. R. Ibarra, *Ultramicroscopy* **2013**, *134*, 144.
[41] L. Jones, H. Yang, T. J. Pennycook, M. S. J. Marshall, S. Van Aert, N. D. Browning, M. R. Castell, P. D. Nellist, *Adv. Struct. Chem. Imaging* **2015**, *1*, 8.

NANO small MICRO

Reprint Order Form 2018
- please return with your proofs -

Editorial Office:

Wiley-VCH Verlag, Boschstrasse 12
69469 Weinheim, Germany

Tel.: (+49) 6201 606 235
Fax: (+49) 6201 606 500

E-mail: advenergymat@wiley-vch.de
http://www.small-journal.com

Manuscript No. _____

Please send me and bill me for

☐ no. of **reprints** via ☐ airmail (+ 25 Euro) ☐ surface mail

☐ **high-resolution PDF file** (330 Euro).

My e-mail address:

_____

Please note: It is not permitted to present the PDF file on the internet or on company homepages

★**Special Offer**★ If you order 200 or more reprints you will get a PDF file for half price.

Information regarding VAT
Please note that from German sales tax point of view, the charge for **Reprints, Issues or Posters** is considered as **"supply of goods"** and therefore, in general, such delivery is a subject to German sales tax. However,this regulation has no impact on customers located outside of the European Union. Deliveries to customers outside the Community are automatically tax-exempt. Deliveries within the Community to institutional customers outside of Germany are exempted from the German tax (VAT) only if the customer provides the supplier with his/her VAT number. The VAT number (value added tax identification number) is a tax registration number used in the countries of the European Union to identify corporate entities doing business there. It starts with a country code (e.g. FR for France, GB for Great Britain) and follows by numbers.

Cover Posters

Posters are available of all the published covers and frontispieces in two sizes

☐ DIN A2 42 x 60 cm/ 17 x 24in (one copy: **39 Euro**)

☐ DIN A1 60 x 84 cm/ 24 x 33in (one copy: **49 Euro**)

Postage for shipping posters overseas by airmail:
+ 25 Euro

Postage for shipping posters within Europe by surface mail:
+ 15 Euro

Mail reprints / cover posters to:

_____
_____
_____
_____
_____

Invoice address:

_____
_____
_____
_____
_____

_____
Date, Signature **Stamp**

VAT no.: _____
(institutes / companies in EU countries only)

Purchase Order No.: _____

Credit Card Payment

VISA, MasterCard, AMERICAN EXPRESS
Please use the Credit Card Token Generator located at the website below to create a token for secure payment. The token will be used instead of your credit card number.

Credit Card Token Generator:
https://www.wiley-vch.de/editorial_production/index.php

Please transfer your token number to the space below.

Credit Card Token Number:

Price list for reprints (The prices include mailing and handling charges. All Wiley-VCH prices are exclusive of VAT)

No. of pages	Price (in Euro) for orders of 50 copies	100 copies	150 copies	200 copies	300 copies	500 copies
1-4	345	395	425	445	548	752
5-8	490	573	608	636	784	1077
9-12	640	739	786	824	1016	1396
13-16	780	900	958	1004	1237	1701
17-20	930	1070	1138	1196	1489	2022
for every additional 4 pages	147	169	175	188	231	315

★ **Special Offer** ★ If you order 200 or more reprints you will get a PDF file for half price.

Wiley-VCH Verlag GmbH & Co. KGaA; Location of the Company: Weinheim;
Chairman of the Supervisory Board: John Kritzmacher,
Trade Register: Mannheim, HRB 432833, General Partner: John Wiley & Sons GmbH,
Location: Weinheim, Trade Register Mannheim, HRB 432296,
Managing Directors: Sabine Steinbach, Dr. Guido F. Herrmann

WILEY-VCH